

5° of latitude, and the thermal wind equation implies a vertical shear of at least 30 m s⁻¹ per scale height (~27 km) in the vortex winds. A temporal sequence of Cassini ultraviolet images showed a large dark oval in the same general location in late October 2000¹³. The feature exhibited a clockwise rotation, and it subsequently moved eastward and deformed. Its connection with the thermal hot spot remains speculative.

The depth to which the hot spot penetrates has not been well determined, but the CIRS data can place limits. Although it is strongly evident in the 1-mbar map, there is an ambiguity as to whether it actually extends down to this level. This is because the spectral region used to obtain the 1-mbar temperatures can be influenced by thermal emission from higher elevations if they are very warm. However, the hot spot is absent approximately one pressure scale height deeper, at the 4-mbar level (Fig. 3b). This sets an upper bound of 4 mbar to the pressure of the spot. □

Received 8 August; accepted 8 October 2003; doi:10.1038/nature02142.

1. Andrews, D. G., Holton, J. R. & Leovy, C. B. *Middle Atmosphere Dynamics* (Academic, New York, 1987).
2. Baldwin, M. P. *et al.* The Quasi-Biennial Oscillation. *Rev. Geophys.* **39**, 179–229 (2001).
3. Orton, G. S. *et al.* Thermal maps of Jupiter: Spatial organization and time dependence of stratospheric temperatures, 1980 to 1990. *Science* **252**, 537–542 (1991).
4. Leovy, C. B., Friedson, A. J. & Orton, G. S. The quasiquadrennial oscillation of Jupiter's equatorial stratosphere. *Nature* **354**, 380–382 (1991).
5. Friedson, A. J. New observations and modeling of a QBO-like oscillation in Jupiter's stratosphere. *Icarus* **137**, 34–55 (1999).
6. Caldwell, J., Tokunaga, A. T. & Gillett, F. C. Possible infrared aurorae on Jupiter. *Icarus* **44**, 667–675 (1980).
7. Caldwell, J. J., Halthore, R., Orton, G. & Bergstralh, J. Infrared polar brightenings on Jupiter. 4. Spatial properties of methane emission. *Icarus* **74**, 331–339 (1988).
8. Drossart, P. *et al.* Thermal profiles in the auroral regions of Jupiter. *J. Geophys. Res.* **98**, 18803–18811 (1993).
9. Gladstone, G. R. *et al.* A pulsating auroral X-ray hot spot on Jupiter. *Nature* **415**, 1000–1003 (2002).
10. Smith, B. A. *et al.* The Galilean satellites and Jupiter: Voyager 2 imaging science results. *Science* **206**, 927–950 (1979).
11. Limaye, S. S. Jupiter: New estimates of the mean zonal flow at the cloud level. *Icarus* **65**, 335–352 (1986).
12. Simon, A. A. The structure and temporal stability of Jupiter's zonal winds: A study of the north tropical region. *Icarus* **141**, 29–39 (1999).
13. Porco, C. C. *et al.* Cassini imaging of Jupiter's atmosphere, satellites, and rings. *Science* **299**, 1541–1547 (2003).
14. Holton, J. R. *An Introduction to Dynamic Meteorology* 3rd edn (Academic, New York, 1992).
15. Kunde, V. G. *et al.* Cassini infrared Fourier spectroscopic investigation. *Proc. SPIE* **2803**, 162–177 (1996).
16. Gierasch, P. J., Conrath, B. J. & Magalhães, J. A. Zonal mean properties of Jupiter's upper troposphere from Voyager infrared observations. *Icarus* **67**, 456–483 (1986).
17. Li, X. & Read, P. L. A mechanistic model of the quasi-quadrennial oscillation in Jupiter's stratosphere. *Planet. Space Sci.* **48**, 637–669 (2000).
18. Magalhães, J. A. *et al.* Zonal motion and structure in Jupiter's upper troposphere from Voyager infrared and imaging observations. *Icarus* **89**, 39–72 (1990).
19. Achterberg, R. K. & Flasar, F. M. Planetary-scale thermal waves in Saturn's upper troposphere. *Icarus* **119**, 350–369 (1996).
20. Deming, D. *et al.* A search for p-mode oscillations of Jupiter: Serendipitous observations of nonacoustic thermal wave structure. *Astrophys. J.* **343**, 456–467 (1989).
21. Deming, D. *et al.* Observations and analysis of longitudinal thermal waves on Jupiter. *Icarus* **126**, 301–312 (1997).
22. Orton, G. S. *et al.* Spatial organization and time dependence of Jupiter's tropospheric temperatures 1980–1993. *Science* **265**, 625–631 (1994).
23. Pallier, L. & Prangé, R. More about the structure of the high latitude Jovian aurorae. *Planet. Space Sci.* **49**, 1159–1173 (2001).
24. Waite, J. H. *et al.* An auroral flare at Jupiter. *Nature* **410**, 787–789 (2001).
25. Beebe, R. *Jupiter* (Smithsonian Institution Press, Washington, 1994).
26. Seidelmann, P. K. *et al.* Report of the IAU/IAG working group on cartographic coordinates and rotational elements of the planets and satellites: 2000. *Celest. Mech. Dynam. Astron.* **82**, 83–110 (2002).
27. Conrath, B. J., Gierasch, P. J. & Ustinov, E. A. Thermal structure and para hydrogen on the outer planets from Voyager IRIS measurements. *Icarus* **135**, 501–517 (1998).
28. Riddle, A. C. & Warwick, J. W. Redefinition of System III longitude. *Icarus* **27**, 457–459 (1976).

Acknowledgements The contributions of T.F. to this work were made while he was at AOP, Oxford University. We thank M. H. Elliott, J. S. Tingley, F. Carroll and M. E. Segura for assistance with instrument commanding and data processing; P. J. Schinder for computing the pointing geometry files for the CIRS observations during the Jupiter swing-by; and D. L. Matson for suggestions.

Competing interests statement The authors declare that they have no competing financial interests.

Correspondence and requests for materials should be addressed to F.M.F. (f.m.flasar@nasa.gov).

Hybridization of electronic states in quantum dots through photon emission

Khaled Karrai¹, Richard J. Warburton², Christian Schulhauser¹, Alexander Högele¹, Bernhard Urbaszek², Ewan J. McGehee², Alexander O. Govorov^{3,4}, Jorge M. Garcia⁵, Brian D. Gerardot⁶ & Pierre M. Petroff⁶

¹Center for NanoScience and Sektion Physik, Ludwig-Maximilians-Universität, Geschwister-Scholl-Platz 1, 80539 München, Germany

²School of Engineering and Physical Sciences, Heriot-Watt University, Edinburgh EH14 4AS, UK

³Department of Physics and Astronomy, Ohio University, Athens, Ohio USA

⁴Institute of Semiconductor Physics, Russian Academy of Sciences, Siberian Branch, 630090 Novosibirsk, Russia

⁵Instituto de Microelectronica de Madrid, CNM-CSIC Isaac Newton, 8, PTM, 28760 Madrid, Spain

⁶Materials Department, University of California, Santa Barbara, California 93106, USA

The self-assembly of semiconductor quantum dots has opened up new opportunities in photonics. Quantum dots are usually described as ‘artificial atoms’, because electron and hole confinement gives rise to discrete energy levels. This picture can be justified from the shell structure observed as a quantum dot is filled either with excitons¹ (bound electron–hole pairs) or with electrons². The discrete energy levels have been most spectacularly exploited in single photon sources that use a single quantum dot as emitter^{3–6}. At low temperatures, the artificial atom picture is strengthened by the long coherence times of excitons in quantum dots^{7–9}, motivating the application of quantum dots in quantum optics and quantum information processing. In this context, excitons in quantum dots have already been manipulated coherently^{10–12}. We show here that quantum dots can also possess electronic states that go far beyond the artificial atom model. These states are a coherent hybridization of localized quantum dot states and extended continuum states: they have no analogue in atomic physics. The states are generated by the emission of a photon from a quantum dot. We show how a new version of the Anderson model that describes interactions between localized and extended states can account for the observed hybridization.

The starting point for our experiments is the generation of excitons with an unambiguous charge in individual self-assembled quantum dots² (see also Supplementary Information). Figure 1 shows the magnetic dispersions of the photoluminescence (PL) from the singly-, doubly- and triply-charged excitons (X^{1-} , X^{2-} and X^{3-} , respectively), all on the same dot. For X^{1-} and X^{2-} , the behaviour is typical of localized excitons. There is a diamagnetic shift arising from the enhancement of the exciton confinement, and a splitting arising from the spin Zeeman effect¹³. However, X^{3-} has a completely different behaviour. At high field, in addition to the spin Zeeman effect, the PL develops a remarkable series of oscillations. This is preceded by a gradual collapse around 1 T of the two low field lines. As we show, the collapse can be explained with the artificial atom model, but the series of oscillations can only be explained with a new electronic interaction.

The X^{3-} PL is represented in Fig. 2 by plotting the energy of each PL peak against magnetic field. Clearly, there is a series of anti-crossings. A number of factors point to an interaction with Landau levels. (Landau levels have energies $E_n = (n + \frac{1}{2})\hbar\omega_c$, where $n = 0, 1, 2, \dots$, and arise when the kinetic energy in an electron band is quantized into units of the cyclotron energy, $\hbar\omega_c$, by a magnetic field.) First, the asymptotes at each anti-crossing are linear

functions of magnetic field, B . Second, the asymptotes for all the anti-crossings extrapolate back to the same energy at zero magnetic field. Third, the PL intensity at each energy is a periodic function of $1/B$. All these features are characteristic of Landau levels in a two-dimensional system. The surprising result is that the PL from an exciton bound to a small quantum dot takes on the

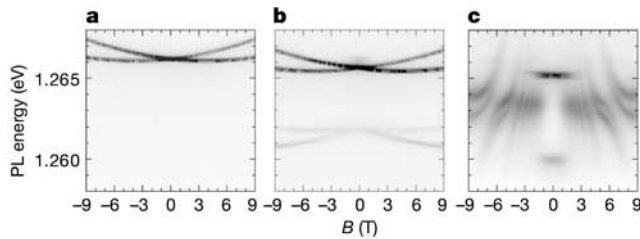


Figure 1 Photoluminescence from charged excitons. Data are shown for singly (a), doubly (b) and triply (c) charged excitons, all from the same quantum dot, versus magnetic field. The photoluminescence (PL) is represented with a grey-scale, and the magnetic field is applied perpendicular to the quantum dot plane. The InAs quantum dots are grown in the Stranski–Krastanow mode on GaAs with an annealing step at the growth temperature in order to increase the ensemble PL energy from 1.1 to 1.3 eV. Under special conditions, the annealing step can lead to the formation of quantum rings. Here, we use the annealing step to form heavily alloyed dots with a vertical height of about 3 nm and a lateral extent of about 40 nm. The heterostructure sequence is GaAs (buffer layer), n^+ -GaAs (back contact), 25 nm GaAs (tunnel barrier), quantum dots, and 150 nm GaAs/AlAs superlattice (blocking barrier). Contacts are made to the n^+ layer and a 5 nm NiCr layer (gate electrode) is deposited on the surface. A voltage V_g is applied between gate and back contact. The sample is mounted into a miniature confocal microscope and cooled to 4.2 K. The PL is excited by non-resonant excitation of the wetting layer with a 830-nm laser diode; the PL is dispersed with a grating spectrometer and detected with a silicon charged-coupled-device camera (spectral resolution 0.1 meV). The excitation power is low enough that any biexciton-related features are much weaker than the exciton PL. The exciton charge can be set unambiguously with the gate voltage because of the strong Coulomb blockade (see Supplementary Information). The neutral exciton is not shown because the shift and splitting in magnetic field are identical to those of the singly charged exciton. The X^{2-} PL has two lines as a consequence of exchange-split final states, one with electron spin $S = 1$, the other with $S = 0$ (ref. 2).

properties of extended states at much higher energies, the Landau levels.

The anti-crossings prove that the quantum dot interacts coherently with the Landau levels. From the splitting at the 6.5-T resonance (2.4 meV), we can deduce that the system oscillates between localized quantum dot character and Landau level character at a frequency of 0.6 THz. The asymptotes shown in Fig. 2 have a negative gradient. Bearing in mind that a PL process involves an initial and a final state, the negative dispersion demonstrates that the hybridization takes place in the final state. In other words, photon emission triggers the hybridization. A resonant interaction with a phonon, a feature in the PL of doped two-dimensional systems¹⁴, can be ruled out because such an interaction would be common to both X^{2-} and X^{3-} , yet in our case, the interaction is completely absent for X^{2-} . We present an explanation of the hybridization based on a purely electronic interaction.

It is important to establish the relative magnitude of the quantization energy and a typical Coulomb energy for the dot studied here. The X^0 diamagnetic shift is both small ($10 \mu\text{eV T}^{-2}$), signifying a strongly confined exciton, and unchanged on charging. This is characteristic of the strong confinement regime where the quantization energy is larger than a typical Coulomb energy¹³. (When the quantization and Coulomb energies are comparable, the diamagnetic shift is larger and decreases significantly on charging¹³.) We reach the same conclusion from the Coulomb blockade. The X^{1-} extends over a much larger gate voltage range than the X^0 and X^{2-} plateaux (see Supplementary Information), demonstrating the large quantization energy. We therefore describe the charged excitons by treating the Coulomb interactions as perturbations to the single-particle states. The dot has s and p orbitals, separated by about 34 meV as deduced from the diamagnetic shift, and we know that the two p orbitals are close to degenerate from the form of the X^{3-} PL at $B = 0$ (explained below). Finally, the d orbitals cannot exist as the X^{3-} is the most highly charged exciton that we can generate before charge occupies not the dot but the wetting layer.

Within the artificial atom model, the X^{3-} emission process is displayed in Fig. 3. The initial state has electron spin $S = 1$ through Hund's rule. When a photon is emitted, there are two possible final

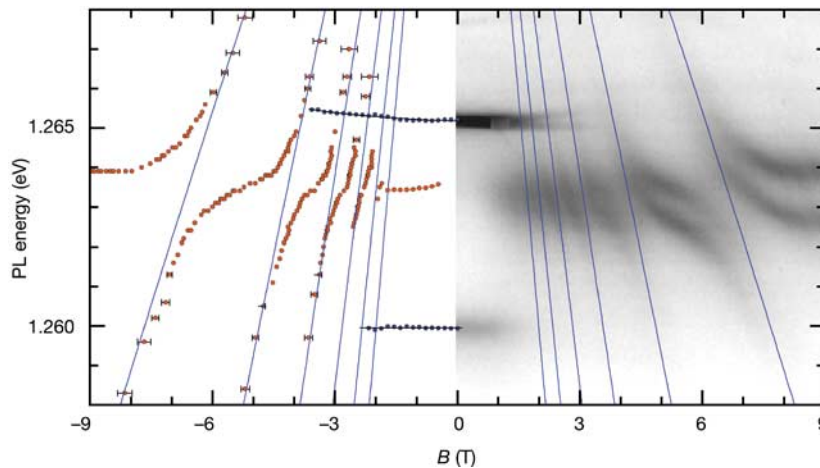


Figure 2 Photoluminescence energy versus magnetic field for the X^{3-} exciton. The points in the plot on the left correspond to the energies of the PL lines shown in Fig. 1c and reproduced on the right. For simplicity, just one spin branch has been included in the plot on the left; the other spin branch shows the same behaviour but shifted in energy. The solid lines show the dependence of energy $E_0 + \Delta - (n + \frac{3}{2})e\hbar B/m_0 m^*$ on magnetic field B with $E_0 = 1.2635 \text{ eV}$, $\Delta = 20 \text{ meV}$ and $m^* = 0.07 - 0.0018|B| + 0.00005B^2$

where Δ is the excess kinetic energy, n the Landau level index, and m^* the effective mass in units of the free electron mass, m_0 . These lines were determined by fitting this functional form to the asymptotes of the anti-crossings. These asymptotes are also shown on top of the original data (right). We note that inclusion of the diamagnetic shift in the analysis does not significantly change the masses that we deduce.

states, $S = 3/2$ and $S = 1/2$, energetically distinct through electron exchange. This is the origin of the two lines in the X^{3-} emission at $B = 0$, the higher- (lower-) energy line corresponding to emission into the $S = 3/2$ ($S = 1/2$) state. A magnetic field introduces an orbital Zeeman splitting between the two p orbitals¹⁵, such that when the splitting exceeds the exchange energy, it becomes energetically favourable for both p electrons to occupy the lower energy p orbital and form an $S = 0$ state¹⁶. We attribute the collapse of the PL splitting around 1 T to this change in configuration. There are two compelling arguments. First, this field can be anticipated from the splitting in the PL at zero field, ΔE . Assuming an isotropic harmonic confinement¹⁷, the configuration change occurs when $\hbar\omega_c = \frac{1}{4}\Delta E$, implying a magnetic field of 0.8 T. This is in good agreement with the experiment where the $S = 1$ and $S = 0$ X^{3-} PL lines have equal intensities at about 1.2 T. Second, once the X^{3-} forms an $S = 0$ state, there is only one possible final state energy, and it is therefore natural for the PL to lie between the two exchange-split lines of the $S = 1$ X^{3-} , exactly as observed. However, within this artificial atom picture, there is no explanation for the anti-crossings that develop at higher magnetic field.

In atomic physics, configurations with the same good quantum numbers and similar energies are admixed. For the $S = 1$ X^{3-} , and also the X^{2-} , the final state configurations involve only the s and p orbitals. However, we find a new possibility for the final state of the $S = 0$ X^{3-} , which has a doubly occupied p orbital and a singly occupied s orbital. We consider first a hypothetical quantum dot with a bound d orbital. The quantum numbers can be preserved by allowing one of the p electrons to fill the vacancy in the s orbital, with the other p electron occupying a higher energy d orbital. These two configurations (Fig. 4a) have the same values of angular momentum and spin and are also almost degenerate, and are therefore admixed. For our dot, the d orbital is unbound so that the mechanism now admixes continuum states to the quantum dot wavefunction (Fig. 4b). The continuum states are associated with the two-dimensional wetting layer. In a magnetic field, the

continuum states are quantized into Landau levels, such that the final state becomes a hybridization of quantum dot states and Landau levels. This means that continuum states impart their character to the PL even though they are never occupied in the initial state. This hybridization occurs for the $S = 0$ X^{3-} but not for the $S = 1$ X^{3-} or the more weakly charged excitons, and there is therefore a close correspondence with the experiments, where the $S = 0$ X^{3-} interacts with the Landau levels but the other excitons do not. Additionally, the interaction takes place in the final state, as required.

The exciton final state is strongly hybridized whenever the energy between the occupied p orbital and the s orbital exactly matches the energy between a Landau level and the p orbital (Fig. 4c). Hybridization with the n th Landau level occurs when $\Delta = (n + \frac{3}{2})\hbar\omega_c$ where Δ is the excess kinetic energy, defined in Fig. 4b ($\Delta = 20$ meV for the dot in Fig. 1). (We have assumed that the p orbital moves down in energy by $\frac{1}{2}\hbar\omega_c$, an exact result for an isotropic and harmonic confinement¹⁵.) As the magnetic field is increased, this condition is satisfied for each Landau level in turn, resulting in the periodicity in $1/B$. Note that hybridization with every Landau level is allowed because every Landau level has a d -like component independent of the Landau level index¹⁸. Ultimately, at high magnetic field (8 T for our particular dot), the interaction with the Landau levels is suppressed because the separation between the s and p orbitals becomes insufficient.

To confirm that our mechanism accounts quantitatively for the experimental results, we have calculated the matrix element $M_n = \langle s^{\uparrow}, p^{\uparrow}, p^{\downarrow} | V_C | s^{\downarrow}, s^{\uparrow}, n^{\downarrow} \rangle$ where $|s^{\uparrow}, p^{\uparrow}, p^{\downarrow}\rangle$ denotes the configuration with two electrons in the lower p orbital and one electron in the s orbital, and $|s^{\downarrow}, s^{\uparrow}, n^{\downarrow}\rangle$ denotes the configuration with two electrons in the s orbital and one in the n th Landau level. V_C is the Coulomb interaction, and \uparrow (\downarrow) denotes spin-up (spin-down). With harmonic oscillator wavefunctions, and Landau level wavefunctions in the

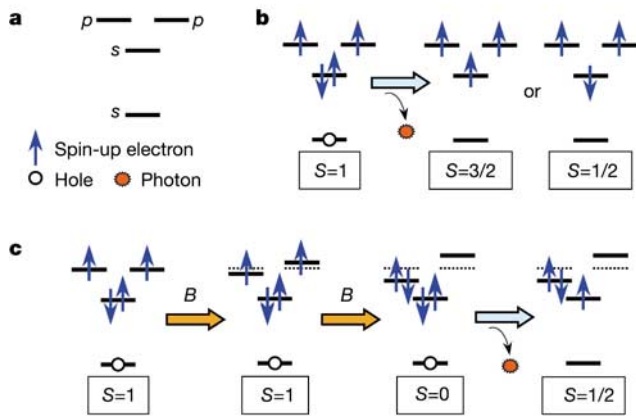


Figure 3 Quantum dot level diagrams in the artificial atom model. **a**, Definition of the orbitals and symbols. Only the lowest-energy hole orbital, labelled s , is shown, as only this hole orbital participates in the recombination. The electron orbitals are labelled s and p with z -component of angular momentum $m = 0, \pm 1$, respectively. Electrons are shown as \uparrow (\downarrow) according to their z -component of spin; the hole has spin $\pm 3/2$. **b**, Configurations are shown for the initial and final states of the triply charged exciton X^{3-} . S refers to the total electron spin in each case. The initial state has $S = 1$. The final state configurations are shown in a simplified way. (The $|S, S_z\rangle = |3/2, 1/2\rangle$ and $|S, S_z\rangle = |1/2, 1/2\rangle$ final states are admixtures of the three configurations in each of which one electron has spin down.) **c**, The initial state configuration change from $S = 1$ to $S = 0$ is shown, induced by a magnetic field.

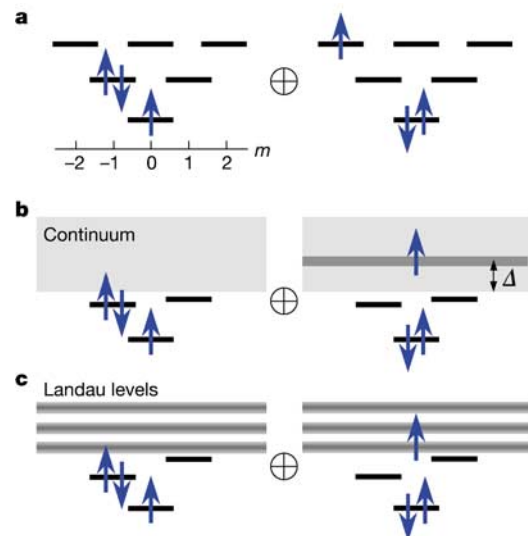


Figure 4 Hybridization in the final state after photon emission. **a**, The artificial atom model including the d orbitals with angular momentum $-2, 0$ and $+2$. The configuration on the left is the final state of the $S = 0$ X^{3-} exciton. It is admixed with the configuration on the right, which has the same spin and angular momentum quantum numbers and almost the same energy. **b**, The admixture when the d orbitals do not exist and there is instead a continuum associated with the two-dimensional wetting layer. The admixture imparts continuum character to the quantum dot exciton. **c**, A large magnetic field is applied to condense the continuum states into Landau levels. The situation shown corresponds to $B = 6.5$ T in the experiment: there is a hybridization of the final state with the $n = 0$ Landau level.

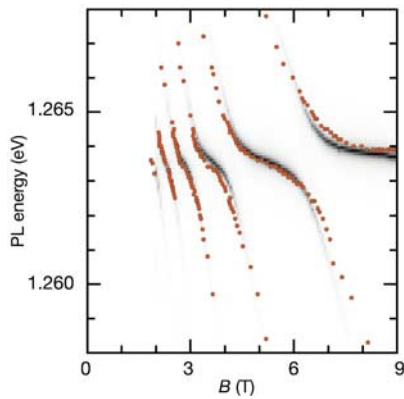


Figure 5 A comparison of the results from the Anderson hamiltonian model with the experiment for the X^{3-} exciton. The grey-scale shows the results of the calculation with the intensity representing the oscillator strength; the points are the same as in Fig. 2 and represent the results of the experiment. Results are plotted with $E_0 = 1.2635$ eV, $\Delta = 20$ meV, $M = 1.2$ meV and $m^* = 0.07 - 0.0018|B| + 0.00005B^2$.

symmetric gauge¹⁸ centred on the dot

$$M_0 = \frac{e^2}{4\pi\epsilon_0\epsilon_r} \frac{16\sqrt{\pi}L_c^3L_c^2(3L_c^2 + L_c^2)}{(2L_c^2 + L_c^2)^{3/2}(6L_c^2 + L_c^2)^{5/2}} \quad (1)$$

where L_c is the characteristic length of the electron wavefunction¹⁷ and $L_c = \sqrt{\hbar/eB}$ is the magnetic length. We determine L_c to be 5.6 nm from the diamagnetic shift of the X^0 PL. At 6.5 T, the field for the resonance with the $n = 0$ Landau level, equation (1) predicts a splitting between the PL lines of $2|M_0| = 2.0$ meV, in very good agreement with the experimental result, 2.4 meV.

The presence of continuum states results in absorption features close in energy to high-energy quantum dot transitions, and because of this the continuum can dephase excited excitons^{19–21}. The mechanism we propose here is significantly different not only because the emission arises from recombination between the lowest-energy electron and hole orbitals, but also because the interaction with the continuum in magnetic field is not a source of scattering but is coherent. We anticipate that the hybridization is by no means unique to our particular quantum dots. The interaction will be a feature for all more highly charged excitons, X^{4-} , X^{5-} , X^{6-} , and so on, because in each case after photon emission, there is a vacancy in the s orbital with a filled p orbital, the necessary requirements for the hybridization to take place. For very deep dots where the d orbital is bound, the interaction will admix d character, but ultimately—for the most highly charged excitons such a dot can support—the exciton energy will lie just below the continuum such that a hybridization with the continuum takes place.

The physics that we are describing is a novel interaction between a localized state and a continuum at higher energy. Such problems are often described by the Anderson hamiltonian²². We have developed a new version of the Anderson model to describe the emission properties of the $S = 0$ X^{3-} . The beauty of this approach is that it relates the optical spectrum, $I(E)$, directly to the density of states in the continuum

$$I(E) \propto \text{Re} \frac{-i}{E - \Sigma(E) - i0}$$

where the self-energy Σ is given by

$$\Sigma(E) = \int_0^\infty \frac{|M(E')|^2 \rho(E') dE'}{E - \Delta + E' - i0}$$

where $M(E)$ is the Coulomb matrix element and ρ the density of

states. Noting that $M(E)$ decreases with increasing energy, we simplify the calculation of Σ by making the approximation that $M(E) = M$, which is a constant for $0 \leq E \leq \hbar^2/(m^* m_0 L_c^2)$, and zero at higher energy. M can be taken from equation (1). However, the theory offers an additional opportunity as we discover that M is related to the linewidth of the $S = 0$ X^{3-} PL at low magnetic field, Γ , and the cyclotron energy at the resonance with the $n = 0$ Landau level, $\hbar\omega_c^0$, through $M = \sqrt{\Gamma\hbar\omega_c^0}/\pi$. The low-field linewidth is $\Gamma = 0.40$ meV, implying $2M = 2.4$ meV, in excellent agreement with the experiment. The results of the calculation, using the experimentally deduced effective mass (Fig. 2), are shown in Fig. 5 and give excellent agreement with the measured X^{3-} PL. This demonstrates conclusively that the hybridization in the experiment is caused by an interaction between localized and extended states, as this is the main content of the Anderson hamiltonian. A natural question is what happens when the wetting layer is filled with electrons. In this case, we find that the $S = 0$ X^{3-} state is favoured even at zero magnetic field (see Supplementary Information), and we anticipate that our new electronic hybridization can coherently couple the quantum dot with the Fermi sea, leading to Kondo-like effects in the emission. \square

Received 23 July; accepted 2 October 2003; doi:10.1038/nature02109.

1. Bayer, M., Stern, O., Hawrylak, P., Fafard, S. & Forchel, A. Hidden symmetries in the energy levels of excitonic 'artificial atoms'. *Nature* **405**, 923–926 (2000).
2. Warburton, R. J. *et al.* Optical emission from a charge-tunable quantum ring. *Nature* **405**, 926–929 (2000).
3. Michler, P. *et al.* A quantum dot single-photon turnstile device. *Science* **290**, 2282–2285 (2000).
4. Moreau, E. *et al.* Quantum cascade of photons in semiconductor quantum dots. *Phys. Rev. Lett.* **87**, 183601 (2001).
5. Yuan, Z. *et al.* Electrically driven single-photon source. *Science* **295**, 102–105 (2001).
6. Santori, C., Fattal, D., Vučković, J., Solomon, G. S. & Yamamoto, Y. Indistinguishable photons from a single-photon device. *Nature* **419**, 594–597 (2002).
7. Gammon, D., Snow, E. S., Shanabrook, B. V., Katzer, D. S. & Park, D. Homogeneous linewidths in the optical spectrum of a single gallium arsenide quantum dot. *Science* **273**, 87–90 (1996).
8. Borri, P. *et al.* Ultralong dephasing time in InGaAs quantum dots. *Phys. Rev. Lett.* **87**, 157401 (2001).
9. Bayer, M. & Forchel, A. Temperature dependence of the exciton homogeneous linewidth in $\text{In}_{0.60}\text{Ga}_{0.40}\text{As}/\text{GaAs}$ self-assembled quantum dots. *Phys. Rev. B* **65**, 041308 (2002).
10. Bonadeo, N. H. *et al.* Coherent optical control of the quantum state of a single quantum dot. *Science* **282**, 1473–1476 (1998).
11. Kamada, H., Gotoh, H., Temmyo, J., Takagahara, T. & Ando, H. Exciton Rabi oscillation in a single quantum dot. *Phys. Rev. Lett.* **87**, 246401 (2001).
12. Zrenner, A. *et al.* Coherent properties of a two-level system based on a quantum-dot photodiode. *Nature* **418**, 612–614 (2002).
13. Schulhauser, C. *et al.* Magneto-optical properties of charged excitons in quantum dots. *Phys. Rev. B* **66**, 193303 (2002).
14. Simmonds, P. E., Skolnick, M. S., Fisher, T. A., Nash, K. J. & Smith, R. S. Hole-quasiparticle resonant polaron coupling in quantum wells containing high densities of free carriers. *Phys. Rev. B* **45**, 9497–9500 (1992).
15. Fock, V. Bemerkung zur Quantelung des harmonischen Oszillators im Magnetfeld. *Z. Phys.* **47**, 446–448 (1928).
16. Tarucha, S., Austing, D. G., Honda, T., van der Hage, R. J. & Kouwenhoven, L. P. Shell filling and spin effects in a few electron quantum dot. *Phys. Rev. Lett.* **77**, 3613–3616 (1996).
17. Warburton, R. J. *et al.* Coulomb interactions in small, charge-tunable quantum dots: A simple model. *Phys. Rev. B* **58**, 16221–16231 (1998).
18. Dingle, R. B. Some magnetic properties of metals I. General introduction, and properties of large systems of electrons. *Proc. R. Soc. Lond. A* **211**, 500–516 (1951).
19. Toda, Y., Moriwaki, O., Nishioka, M. & Arakawa, Y. Efficient carrier relaxation mechanism in InGaAs/GaAs self-assembled quantum dots based on the existence of continuum states. *Phys. Rev. Lett.* **82**, 4114–4117 (1999).
20. Kammerer, C. *et al.* Photoluminescence up-conversion in single self-assembled InAs/GaAs quantum dots. *Phys. Rev. Lett.* **87**, 207401 (2001).
21. Vasanelli, A., Ferreira, R. & Bastard, G. Continuous absorption background and decoherence in quantum dots. *Phys. Rev. Lett.* **89**, 216804 (2002).
22. Hewson, A. C. *The Kondo Problem to Heavy Fermions* (Cambridge Univ. Press, Cambridge, 1993).

Supplementary Information accompanies the paper on www.nature.com/nature.

Acknowledgements We acknowledge discussions with A. Rosch and J. von Delft. This work was funded by the DFG, EPSRC and The Royal Society.

Competing interests statement The authors declare that they have no competing financial interests.

Correspondence and requests for materials should be addressed to R.J.W. (R.J.Warburton@hw.ac.uk).